

# Fluorescence enhancement in large-scale self-assembled gold nanoparticle double arrays

M. Chekini,<sup>1)</sup> R. Filter,<sup>2)</sup> J. Bierwagen,<sup>1)</sup> A. Cunningham,<sup>1)</sup> C. Rockstuhl,<sup>3,4)</sup> and T. Bürgi,<sup>1a)</sup>

<sup>1</sup>*Département de Chimie Physique, Université de Genève, 1211 Genève, Switzerland.*

<sup>2</sup>*Institute of Condensed Matter Theory and Solid State Optics, Abbe Center of Photonics, Friedrich-Schiller-Universität Jena, D-07743 Jena, Germany*

<sup>3</sup>*Institute of Nanotechnology, Karlsruhe Institute of Technology, D-76021 Karlsruhe, Germany*

<sup>4</sup>*Institute of Theoretical Solid State Physics, Karlsruhe Institute of Technology, D-76131 Karlsruhe, Germany*

Localized surface plasmon resonances excited in metallic nanoparticles confine and enhance electromagnetic fields at the nanoscale. This is particularly pronounced in dimers made from two closely spaced nanoparticles. When quantum emitters, such as dyes, are placed in the gap of those dimers, their absorption and emission characteristics can be modified. Both processes have to be considered when aiming to enhance the fluorescence from the quantum emitters. This is particularly challenging for dimers, since the electromagnetic properties and the enhanced fluorescence sensitively depend on the distance between the nanoparticles. Here, we use a layer-by-layer (LBL) method to precisely control the distances in such systems. We consider a dye layer deposited on top of an array of gold nanoparticles or integrated into a central position of a double array of gold nanoparticles. We study the effect of the spatial arrangement and the average distance on the plasmon-enhanced fluorescence. We found a maximum of a 99-fold increase in the fluorescence intensity of the dye layer sandwiched between two gold nanoparticle arrays. The interaction of the dye layer with the plasmonic system also causes a spectral shift in the emission wavelengths and a shortening of the fluorescence life times. Our work paves the way for large-scale, high throughput, and low-cost self-assembled functionalized plasmonic systems that can be used as efficient light sources.

## I. INTRODUCTION

Field enhancement close to metal nanoparticles, due to their localized surface plasmon resonances (LSPR) found a plethora of applications in enhanced spectroscopy.<sup>1-7</sup> These particles are usually considered as a nanoantenna that enhances luminescence, fluorescence, and Raman scattering signals.<sup>2-4,7-11</sup> Fluorescence labelling, sensing, and imaging are popular techniques with applications in chemistry and biology.<sup>1,2,8,12-14</sup> Favourable fluorescent materials for efficient light sources, biological labelling, imaging, and sensing should exhibit certain emission properties, i.e. concerning photostability, brightness, and efficiency.

---

<sup>a)</sup> Author to whom correspondence should be addressed, E-mail: Thomas.Buergi@unige.ch

The emission properties of commonly-used fluorescent materials (e.g. fluorescent dye molecules or fluorophores) are not intrinsic but can be improved by modifying the optical environment the fluorescent materials perceive. This led to the development of metal-enhanced fluorescence approaches.<sup>7,9,10,12-20</sup>

Generally, the fluorescence can be altered by nearby metallic nanoparticles through different means. To appreciate the opportunities but also the delicate interplay, we stress that fluorescence is a process where a high-energy photon is first absorbed by the fluorophore that is excited from its ground state to a higher-level excited state. Second, a nonradiative decay occurs to a lower lying excited level. And third, a radiative decay occurs to the ground state accompanied by the emission of a low energy photon. Besides the nonradiative decay that is intrinsic to the molecule, the first and the third step can be strongly influenced by the optical environment.

First, near-field enhancements close to the nanoparticles enhance the incident optical intensity at the spatial position of the fluorophore. This enhances absorption. Since the LSPR are evanescent in nature, the enhancement is strongest close to the interface. Therefore, smaller distances suggest an enhanced absorption by the fluorophore.<sup>2,18,21,22 14,18,23,24</sup>

Second, the radiative decay rate of the fluorophore can be increased in the vicinity of nanoparticles. This increases its emission and influences its quantum yield, shortens the fluorophore life time, and improves its photostability by reducing the chances of photo-bleaching.<sup>12-14,18,19,23-27</sup> The increase in decay rate occurs because the excited fluorophores do not just couple to the free space modes. In close vicinity to the nanoparticle they can also couple to the plasmon mode. Once excited, the lowest order plasmonic modes that are electric dipolar in nature can couple very well to the far-field. This enhances the emission rate.<sup>15,28,29</sup> Therefore, it is again suggested that the distances between nanoparticles and fluorophores are as small as possible.

However, if the dye is located at a metallic surface or its very close vicinity, charge or energy transfer processes that is non-radiative decay may occur which quenches the emission. Moreover, the plasmon mode is characterized not just by a radiative but also by non-radiative losses. This is less severe for larger distances between the nanoparticle and the fluorophore where the coupling usually occurs to the electric dipolar plasmon mode. But for excessively small distances the coupling occurs also to higher order plasmonic modes that are optically dark. Losses of dark modes are predominantly non-radiative, which reduces the emission. All together this leads to a strong quenching of the fluorescence instead of its enhancement.<sup>1,12-15,22</sup>

As a result and considering the concerted action of all processes, there is an optimal distance for the fluorophore from the particle's surface to maximize the fluorescence.<sup>12,16,19,21,26,30</sup> Therefore, it is essential to control the distance between the

fluorophores and the particles surface.<sup>12,14,16,19,21,26,31</sup> In order to achieve such distance control, the use of different types of spacers have been reported such as silica<sup>22,24,32-35</sup>, polymers<sup>7,19,21,36-39</sup>, and biomolecules.<sup>28,40-42</sup>

However, one important factor is yet unconsidered. The spectral agreement between the transition frequencies of the fluorophores and the resonance frequencies of the plasmon mode where all aforementioned effects are maximized. Since in the weak coupling regime, which we consider here, the transition frequencies of the fluorophores are fixed, the spectra of the LSPR can be tuned and tailored by changing the geometry of the metal nanoparticle sample. Moreover, the balance between the radiative and non-radiative losses of LSPR depends equally on geometrical details (particle size, shape and spacing). The non-radiative decay, e.g., dominates for small nanoparticles and excludes their consideration for fluorescence enhancement. In contrast, LSPRs of larger particles are dominated by radiative losses that efficiently enhance fluorescence.<sup>12,18,42-44</sup>

In closely spaced nanoparticles (dimer configuration), all these processes depend additionally on the nanoparticle spacing. For example, the hybridization of the LSPR of two isolated nanoparticles shifts the resonance frequency of the bright mode depending on the size of the gap.<sup>43,45-48</sup> Thinner gaps result in stronger hybridization. The dimer configuration thus gives better plasmon resonance tunability than a single particle. It also provides a better enhancement of the field that is localized between the closely-spaced particles.<sup>23,25,30,39,42,43,48-51</sup> Hence, if fluorophores are located inside such narrow gaps, their absorption can be drastically enhanced.<sup>14,30,40,43,49-53</sup> Furthermore, the emission properties are increased since such dimer configurations usually exhibit much better radiation efficiencies due to the reciprocity theorem.<sup>54</sup> All these processes as sketched above are basically understood when considering single nanoparticles or dimers. However, if those processes shall be exploited in novel light sources, they have to be studied at the level of larger ensembles in solid phase<sup>43</sup> similar to the studies in solution phase<sup>30,50,51,55</sup>. Then, ideally, also the plasmonic substrate shall be fabricated by a cheap, reliable, and fast technology that enables one to obtain the desired structures on large scales with precise control over the geometry.

Here, we exploit the layer-by-layer (LBL) method to realize large-scale self-assembled arrays of nanoparticles for fluorescence enhancement. Our method is based on the sequential adsorption of oppositely charged polyelectrolyte (PE) to build up multilayers of very well defined distances. This approach is very well suited to set a minimum distance between the fluorescent layer and the gold nanoparticles, since the thickness of the multilayer film increases linearly with the number of deposited bilayers.<sup>26,39,46,56-59</sup> This versatile method is simple, well-established, and can be carried out at room temperature and on a variety of substrates.<sup>26,39,45,60,61</sup> The charged PE-coated surface is suitable to incorporate charged species such as metal nanoparticles and to introduce a buffer layer or barrier between them.<sup>26,39,45,60,61</sup> Particularly, we study not just isolated arrays of nanoparticles on which we deposit fluorophores and their distance dependent fluorescence, we also study the incorporation of the fluorophores into a central position of coupled arrays of gold nanoparticles. Even though an exact

correlation of the spatial position of nanoparticles in adjacent arrays is not possible, we witness a strong coupling between particles in the upper and the lower arrays. This coupling requires considering the formation of nanoparticle dimers to fully understand the optical response of the plasmonic substrate. Since we incorporated fluorophores into the gap of those dimers, we can explain the tremendous fluorescence enhancement by two orders of magnitude, which we observe experimentally in optimal samples.

In our work we investigate the enhancement of the fluorescence emission of two fluorescent dyes with emission bands around 650 nm (CF<sup>TM</sup>620R) and around slightly longer wavelengths (Nile blue A [NB]) in the presence of self-assembled gold nanoparticle (AuNP) arrays. We show that these plasmonic structures can be effectively used to enhance the fluorescence of near-infrared (NIR) fluorescent dyes. Several samples were prepared through self-assembly of AuNPs at a glass surface. Using the LBL method we obtained nanometer range spacers between the particle arrays and the dye layer from zero nanometers (no layer) up to several tens of nanometers. The successful use of the layered structure to introduce defined distances between the dye and nanoparticles, and also to prevent diffusion of the dye, is confirmed by Raman measurements. We conduct fluorescence and lifetime measurements. The averaged fluorescence enhancement of the dye as a function of distance to the particle array in single and double array configurations is investigated. We reached enhancement factors up to two orders of magnitude.

## **II. EXPERIMENTAL**

### **A. Preparation of colloidal AuNPs**

We used the conventional Turkevich method to prepare colloidal solutions of AuNPs.<sup>62</sup> Size alteration of the AuNPs can be obtained by changing the ratio of citrate to gold salt concentration. However for larger particles, a less uniform shape and size is realized.<sup>63,64</sup> We prepared AuNPs with approximate diameters of 40-60 nm. To do so, gold salt solution (600 mL of  $2.5 \times 10^{-4}$  M) was brought to 100°C under constant stirring in an oil bath. Introducing 7.5 mL of a 0.03 M sodium citrate solution to the boiling gold salt solution reduced the gold ions. The solution was kept at 100°C for further 30 minutes before removing from the oil bath and cooling down to room temperature.<sup>62,64</sup>

### **B. Functionalization of glass substrates**

Glass slides were carefully cleaned with piranha solution (3 to 1 mixture of concentrated sulphuric acid and 30% hydrogen peroxide; piranha solution is dangerous and should be handled carefully). Later the slides were immersed in 5% solution of N-[3-(Trimethoxysilyl)propyl]ethylenediamine in ethanol for 30 minutes. Aminosilane groups were attached to

the surface due to organosilane interaction with surface Si atoms, followed by Si-Si polymerization. The glass slides were rinsed several times with copious amounts of Milli-Q water to remove unattached species and dried under the stream of compressed air. The slides were cured for 30 minutes at 120 °C to covalently bind the aminosilane groups to the surface Si atoms.

### **C. AuNPs adsorption on glass slides**

Each functionalized glass slide was immersed in 25 ml of AuNP solution for 90 minutes under static condition. Electrostatic interaction lead to spontaneous adsorption of negatively charged citrate stabilized AuNPs on the positively charged aminosilane functionalized glass slides. The density of adsorbed nanoparticles gradually increased with time and an amorphous layer is formed on the glass surface. The samples were rinsed with excess of water and dried under the stream of dry air after removing from the AuNP solution.

### **D. Polyelectrolyte spacer and dye layer deposition**

We prepared several samples with different spacer thickness through the layer-by-layer bottom-up approach similar to a recently described method.<sup>31</sup> After deposition of the first AuNP array, several sequences of positively and negatively charged PE layers (PAH: poly(allylamine hydrochloride) and PSS: poly(styrene sulfonate)) were deposited by dip-coating in 5 mg/mL aqueous solution of sodium chloride ( $10^{-1}$  M) for one minute. After each PE deposition step, the samples were rinsed carefully with milli-Q water and dried under the stream of compressed air. Several samples were prepared differing in the number of PE bilayers. A schematic view of the preparation procedure is presented in Fig. 1. The sample composition can be denoted as AuNP-PAH-(PSS-PAH)*i*-dye layer; The index *i* shall represent the number of introduced PE bilayers that are later used to separate the lower AuNP array and the dye layer in each sample. For NB dye, samples with *i* = 0, 1, 2, ..., 8, 10, 15, and 20 were successfully assembled. For CF<sup>TM</sup>620R, samples with *i* = 0, 1, 2, ..., 8, 10, 15, 20, 30, and 40 were prepared.

After building up *i* PE bilayers on top of the first AuNP array, the dye layer was deposited. In the case of samples with CF<sup>TM</sup>620R as a dye, each sample was dipped in 37.8 μM aqueous solution of free acid dye for 1 minute for electrostatic driven adsorption of the dye, followed by rinsing with milli-Q water and drying. For preparation of the samples with NB as a dye, samples were immersed in 50 μM aqueous solution of dye for 1 minute, followed by a washing and a drying step. Subsequently, the samples were immersed in 5 mg/mL PSS in  $10^{-1}$  M aqueous solution of sodium chloride and 5 μM dye for 1 minute, washed, and dried again. Addition of dye at this step is necessary to compensate its desorption from the sample. The same procedure (dipping in dye and PSS solution) was repeated once to increase the dye adsorption. Another set of

barrier bilayers (i PE bilayers) was then deposited on top of the dye layer before the second (the upper) AuNP array deposition. The second AuNP array was deposited on the final positively charged PAH layer, which concludes the formation of the nanoparticle double array as shown in Fig. 1. The reference samples were prepared in a similar way on glass slide (without AuNP array and  $i = 5$ ).

## E. Characterization

Ultraviolet-visible and near-infrared spectroscopy was carried out on a Jasco V-670 UV-Vis/NIR spectrophotometer. Scanning electron microscopy (SEM) measurements were conducted on a SEM JEOL 7600F system with 2.00 kV acceleration voltage. The samples were coated by gold sputtering prior to these measurements.

## F. Numerical calculations

In the numerical calculations we aim to simulate the extinction cross section that is also experimentally measured. The challenge in the simulation is the enormous number of degrees of freedom of the system under consideration: the properties of the impinging light field (polarization, direction, statistical properties), the actual orientation of all the AuNPs against each other (displacements in x-, y-, and z-coordinate), and the physical parameters of the quantum system (actual polarization of the excitation, near-field coupling to adjacent molecules etc.), just to name a few. A brute-force approach that takes most of these parameters for a simulation into account is impossible. As a reasonable approximation and with the purpose to calculate only the extinction cross section, therefore, we employed a simplified electromagnetic model of the AuNPs to describe the scattering of an ensemble of particles with just two parameters: a separation distance depending on the number of PE layers and a filling fraction  $f$  that accounts for the amount of dimer configurations in the ensemble. The remaining fraction is considered as isolated nanoparticles.

The separation distance is given by lateral and vertical distances  $d_x$  and  $d_z$  respectively. Because of the fabrication method, the vertical distance  $d_z$  is given by the thickness of the PE layers. Furthermore, the minimum lateral distance  $d_x$  between the centers of the spherical AuNPs is given by their diameter plus the thickness of the applied PE layers. The filling fraction  $f$  is used to interpolate between a pure-dimer realization ( $f = 1$ ) and single spheres ( $f = 0$ ). In this approximation, the extinction cross section ( $\sigma^{tot}(\lambda, d_z)$ ) is calculated as:

$$\sigma^{tot}(\lambda, d_z) = f \sigma^{dimer}(\lambda, d_z) + (1 - f) \sigma^{single}(\lambda)$$

This extinction model assumes a linear superposition of single particle and dimer configurations to the ensemble's response. Even if it is a very crucial approximation, the model allows to investigate the contributions of dimer and single sphere modes to the ensemble's interaction with an external driving field.

All numerical calculations have been performed with an in-house code that solves the general Mie problem for a multiple number of spheres. With that method we calculate the extinction cross section of the dimer and the single particle depending on the wavelength and, for the dimer, the thickness of the PE layer as indicated above.<sup>65</sup> Because of the parameters of our fabrication process we assume a diameter of 40 nm for the AuNPs in our simulations. Furthermore it is assumed that the particles are placed inside a dielectric with a certain refractive index (e.g.  $n = 1.5$  for fully embedded particles). This takes the linear response of the PE layers to the electromagnetic driving field approximately into account. Material properties of gold as documented in literature were taken into account.<sup>66</sup> The incident electric field has been polarized parallel to the dimer axis. The spectra of the opposite polarization, i.e. perpendicular to the dimer axis, is nearly indistinguishable to the spectra of the isolated sphere, something we took into account in the averaging procedure described above.

## **G. Fluorescence emission and life time measurements**

We used the commercially available fluorometer Fluorolog 3 from Horiba for the fluorescence emission measurements. The lifetime was measured with a custom made setup. A white light laser (NKT, SuperK EXW-12) was utilized for excitation. For the wavelength selection an AOTF-based system (NKT, SuperK Varia), combined with appropriate band pass filters was used, to suppress undesired wavelengths in the excitation light. The samples were excited with the laser light by focusing it onto the sample. The fluorescence light was cleaned from excitation light with appropriate long pass filters and collected with a 1:1 telescope in an orthogonal geometry and refocused into a multimode fiber bundle (LOT, circular to rectangular LLB552). The fiber delivered the light to a monochromator (Horiba Jobin Yvon, Triax190), with which the residual excitation light was eliminated and the relevant spectral region could be selected to measure the fluorescence life time. The light was detected with a PMT (PicoQuant, PMA-C 192-N-M) and the detected events were correlated (PicoQuant, PicoHarp300) with the excitation pulse signal from the laser. For collecting the data each sample was measured for 200 seconds. After the experiment the instrument response function (IRF) was measured to perform the deconvolution in the following analysis.

## **H. Lifetime estimation**

The lifetime for each sample was estimated by the deconvolution method using the system identification toolbox of MATLAB R2014a. In order to compute the lifetime, first the inputs (IRF) and outputs (measured fluorescence decay) were used to identify a linear convolutional model for each sample such that the output of each model is the result of convolving the excitation with the impulse response of that model. The impulse response is the system output when the input is an ideal impulse (Dirac delta).<sup>67</sup> The reported lifetime of each sample is represented by an exponential decay in the sample impulse response.

## I. RAMAN MEASUREMENTS

A custom-made setup was used for Raman measurements. For excitation, a HeNe-Laser with a wavelength of 632.8nm (JDSU, Model 1144) was used and unwanted sidebands were removed with a clean-up filter (AHF Analysentechnik, HC Laser Clean-up MaxLine), which was placed in the beam path. The Raman light was collected and refocused with a 1:1 telescope and sent into a spectrograph (Kaiser Optics-Systems, HoloSpec VPT). A Notch-filter (Kaiser Optics-Systems) suppressed the excitation light before the dispersed beam was prompted onto a liquid nitrogen cooled CCD-camera (Princeton Instrument, LN/CCD-1792-PB). The whole setup was controlled via a custom-made program.

## III. RESULTS AND DISCUSSION

The sample preparation procedure is schematically depicted in Fig. 1 and Fig. 2 shows a SEM image of a double AuNP double array. We synthesized AuNPs with approximate diameter of 40-60 nm. The plasmon resonance of larger particles are more red-shifted<sup>12,18,44</sup> and more suitable for enhancing the fluorescent of NIR dyes due to the better overlap of the emission with the excitation wavelength. The samples were prepared with two different fluorescent dyes (CF<sup>TM</sup>620R and NB). We first discuss results obtained with CF<sup>TM</sup>620R.

The extinction and fluorescence emission of the samples with CF<sup>TM</sup>620R as a fluorescent dye have been measured in two configurations, i.e. single array of nanoparticles with the dye layer on top and double array of nanoparticles with the sandwiched dye layer (Fig. 1).

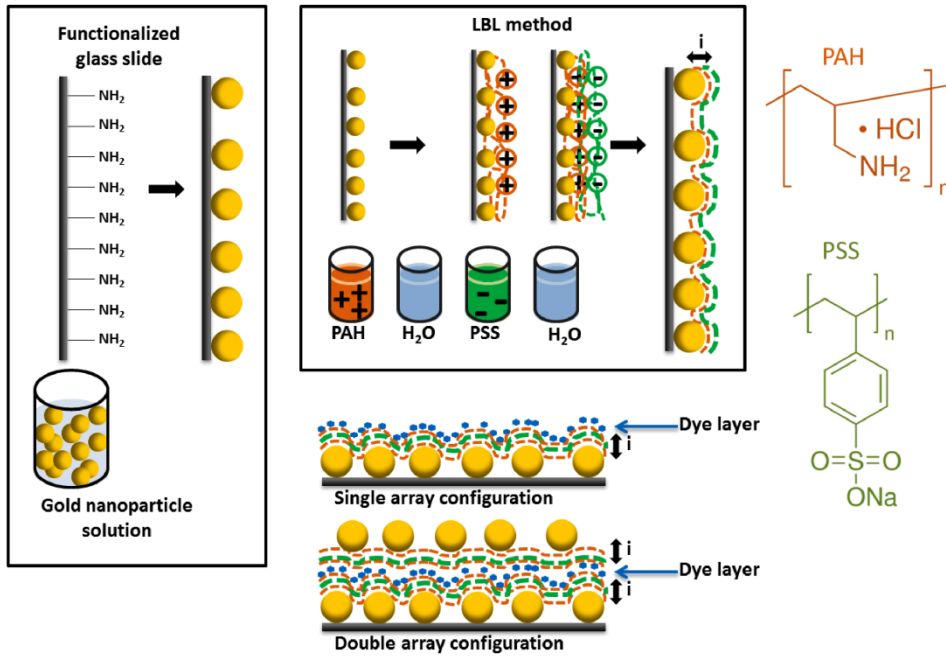


Fig. 1 Schematic view of samples preparation. In a first step the AuNPs were deposited on amino functionalized glass slides. In order to introduce barrier layer, different numbers of PE bilayers were deposited by LBL method. To form double array configuration, the same number of PE bilayers were deposited on the dye layer before deposition of the second AuNP array.

The extinction spectra of the samples with a single array of nanoparticles are shown in Fig. 3a. They show a red-shift of the plasmon resonance with an increasing number of PE bilayers. This shift is due to the change of the particles environment and the increasing coverage of the AuNP array by the PE layers that has a higher refractive index than air (see figure S1 of the supplementary material<sup>68</sup>).<sup>31,45</sup>

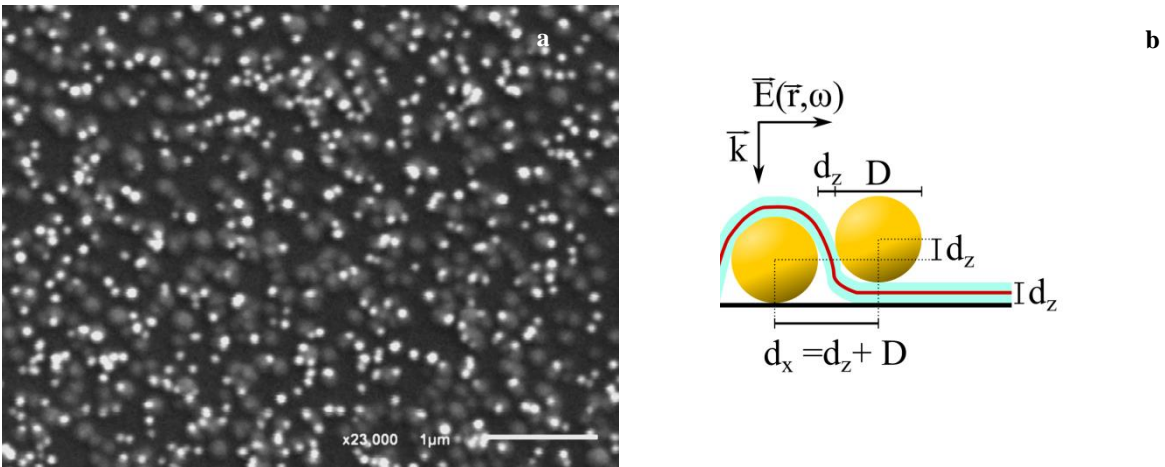


Fig. 2 SEM micrograph of sample i30, with 60 PE bilayers separating the bottom and top nanoparticle arrays (a). The shiny particles with high contrast are the top array nanoparticles and the blurred bumps are bottom array nanoparticles buried in PE layers. Scheme of the possible dimer arrangements formed in samples and used for calculations of dimer extinction cross section (b).  $k$  and  $E$  are the incoming light's wave vector and polarization of electric field.  $d_x$  and  $d_z$  indicate the lateral and vertical separation of nanoparticles (with diameter  $D$ ).  $d_z$  is defined by the thickness of the PE layer.<sup>46</sup>

The larger the refractive index of the surrounding material, the larger the red-shift. This explanation is fully supported by numerically calculated extinction spectra of gold spheres embedded in air and a dielectric with  $n = 1.5$  (Fig. 3c).

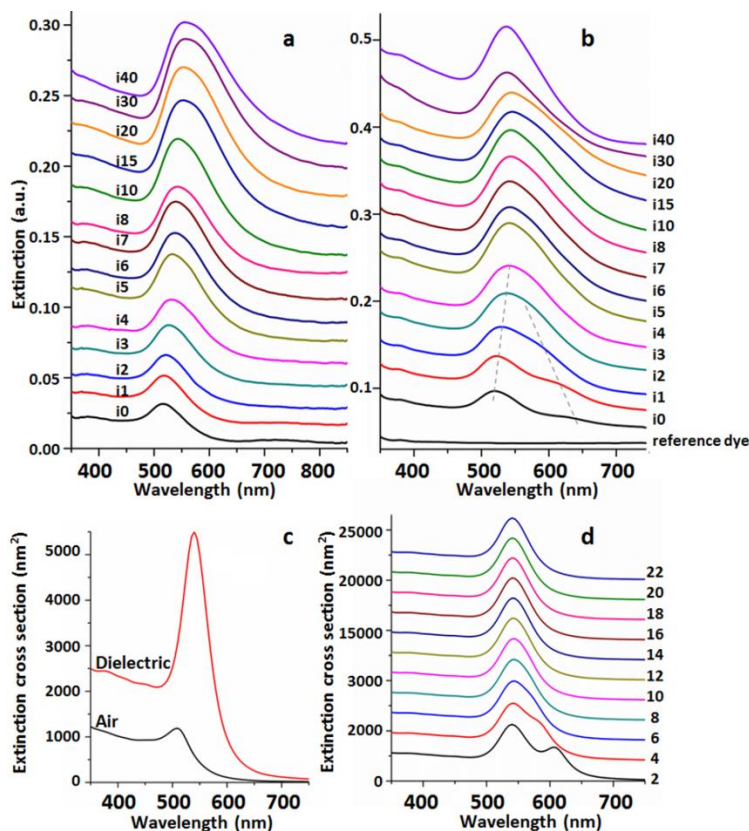


Fig. 3 Extinction spectra of single AuNP array (a) and double AuNP array (b) with different number of PE bilayers. The second peak due to coupling between nanoparticles in two arrays (some dimer configurations) appears at small separation distances. By increasing the numbers of barrier layers, the plasmon resonance peak red-shifts from 522 to 545 nm and also broadens. Calculated extinction cross sections for a single gold sphere embedded in air (black line) and a dielectric with  $n = 1.5$  (red line) (c). Predicted extinction spectra by a mixing rule as described with  $f = 0.15$  for separation distances from 2 to 22 nm (d).

In order to form a double array configuration with the sandwiched dye, the same numbers of PE barrier layers were deposited between the lower AuNP array and the dye layer, and between the dye and the upper AuNP array, as depicted in Fig. 1. Fig. 2 shows an SEM micrograph of the i30 sample with overall 60 separating PE bilayers. The lower nanoparticle array appears more blurred and has less contrast due to the embedding in the PE layers. The brighter high-contrast particles correspond to the upper nanoparticle array. Formation of some nanoparticle dimers with a minimum separation, defined by the number of PE layers, is expected in these samples. Fig. 3b shows the UV-Vis extinction spectra of the double array samples. The spectrum for i1 clearly shows a second peak at 620 nm due to the coupling of the two nanoparticle arrays (dimer formation). Note that formed dimers with the dimer axis oriented perpendicular to the surface do not contribute to the longitudinal plasmon resonance<sup>43</sup>, and therefore the second peak at longer wavelength is rather weak. The second peak is also blue shifted and merged to the red-shifted first plasmon resonance peak by increasing the separating barrier thickness to 6 PE bilayers (i3 sample). A red-shift and a broadening of the plasmon resonance (first peak) is observed by further

increasing the separation between the two particle arrays. This shift persists until 15 PE bilayers as a result of the increased refractive index surrounding the particles (see figure S1 of the supplementary material<sup>68</sup>).<sup>31,45</sup> Further increasing the barrier thickness leads to weakening of coupling between the two particle arrays and as a result a slight blue shift in extinction spectra (i20, i30 and i40 at Fig. 3b).

The numerical prediction is more complex for the double array configuration. Because of the random arrangement of the nanoparticles, different geometrical configurations contribute to the extinction. Hence, in contrast to the realized geometries in a former work<sup>46</sup>, the extinction cross section has been considered here as being composed of a contribution by single and dimer configurations. The extinction cross sections of AuNps dimers have been calculated for different separation distances (PE barrier thickness changing from 2 to 22 nm) by considering  $d_x$  and  $d_z$  as lateral and vertical separations (Fig. 2), which are defined as  $d_z$  = PE barrier thickness and  $d_x$  = PE barrier thickness + diameter (40 nm).

The characteristics of the extinction can be understood if a statistical combination of single and dimer-configurations is considered, as described by the filling factor (see experimental section). For  $f = 0.15$ , we find a good agreement to the experimentally determined extinction (Fig. 3). From Fig. 2 is evident that the sample does not only consist of single (isolated) particles and dimers, but also of larger aggregates. However, the essence of the extinction spectra can be reproduced by a model comprising single particles and dimers.

The emission spectra of the different CF<sup>TM</sup>620R samples were measured with an excitation at 550 nm (see figure S2 of the supplementary material<sup>68</sup>). For all samples with a single AuNP array, except i0, a reduction of fluorescence was observed with respect to the reference dye sample ( $i = 5$ ). The sample i0 with the dye at closest distance to the nanoparticles (one PAH barrier layer) showed a slight fluorescence enhancement of about 1.7-fold as shown in Fig. 4.

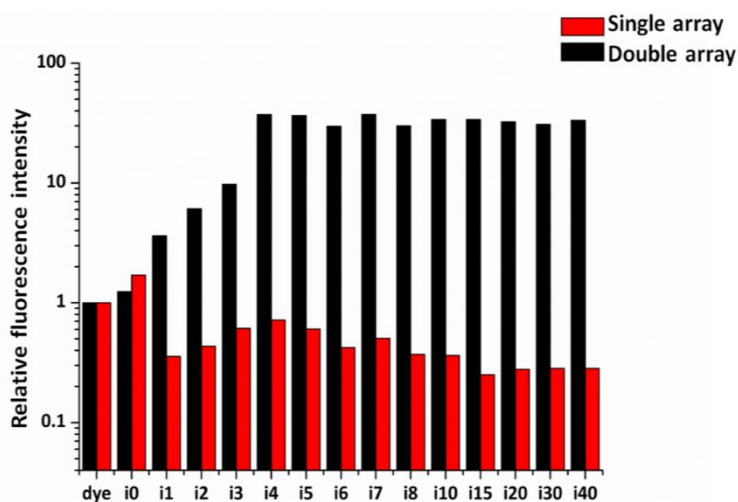


Fig. 4 Relative fluorescence enhancement (normalized to reference dye sample  $i = 5$ ) of the samples with CF<sup>TM</sup>620R dye with excitation at 550 nm for single AuNP array (red) and double array (with some dimer configuration), black.

The decrease in fluorescence intensity of the dye has been experimentally and theoretically reported when the distance from a single AuNP increased.<sup>30,49</sup> These studies demonstrated the occurrence of decreased fluorescence intensity at a certain distance due to quenching. In our example this is the case for sample  $i1$ . After that the fluorescence increases again. However, for all samples except  $i0$  we still encounter quenching effects since the separation distances are comparable to the size of the nanoparticles.

The measured fluorescence enhancement of the double array configuration with an excitation at 550 nm shows a different behavior. Fig. 4 shows the relative peak heights of emission spectra (normalized to reference dye sample  $i = 5$ ) of the double array samples (the emission spectra are presented in figure S3 of the supplementary material<sup>68</sup>). Due to differences in electromagnetic near field distributions, there is a difference of fluorescence enhancement for single particle and dimer configuration as is evident from Fig. 4. In single particle configuration, we observed enhancement only for the sample with the dye as close as 1 single PE layer ( $i0$ ). However for the double array configuration, there is an enhancement in fluorescence by increasing the barrier layers until the sample  $i4$ . For samples with thicker barriers, the fluorescence is 37-fold enhanced compared to the reference dye sample. This enhancement and saturation behavior can be explained by the yet low absorption of the dye at the excitation wavelength. It is expected that it can be improved if the absorption process is driven at slightly longer wavelengths where there is a better overlap with plasmon resonances.

To confirm this, the fluorescence enhancement behavior in the same double array samples was further investigated by exciting at 590 nm. At this longer wavelength the dye absorbs more light and there is still a good overlap with the plasmon resonance of the double array AuNPs samples. Another set of double-array samples with NB as a dye was prepared. The corresponding extinction spectra of these samples are shown in figure S4 of the supplementary material<sup>68</sup>. We discuss in the following at first double array samples with NB and later CF<sup>TM</sup>620R as a dye.

The fluorescence emission spectra and corresponding enhancement factors for NB dye are shown in figure S5 of the supplementary material<sup>68</sup> and Fig. 5, respectively. As shown there, no enhancement is observed for the samples  $i0$ ,  $i1$ , and  $i2$  for the NB samples. Slight quenching is even observed in these samples, due to the very close distance between NB and the AuNPs' surfaces (estimated to be less than 2.5 nm by ellipsometry). By increasing the number of PE bilayers (larger  $i$ ), we observed a notable enhancement in fluorescence emission until reaching an optimal distance. The maximum enhancement is observed for the  $i7$  sample with a 17.6-fold enhancement compared to the NB dye reference sample. For even thicker barrier thicknesses the fluorescence enhancement gradually decreases, reaching 11-fold enhancement for  $i15$  and  $i20$ . The optimum distance can be explained by two competing effects: field enhancement and quenching. At the optimal distance ( $i7$ ) the field

enhancement largely over-compensates quenching. By further increasing the spacer thickness beyond the optimal value, the coupling between the nanoparticle arrays weakened and the near-field intensities between the particles decreases. This led to a drop of fluorescence enhancement.

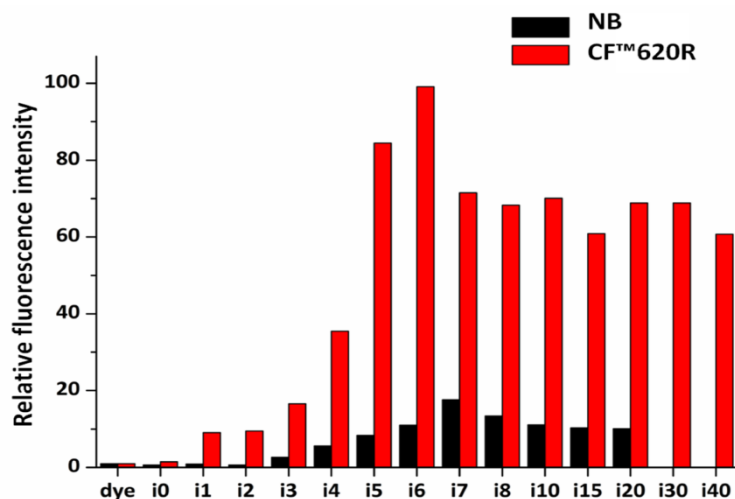


Fig. 5 Relative fluorescence enhancement (normalized to reference dye sample  $i = 5$ ) with excitation at 590 nm for NB double array samples (black) and CF™620R samples (red). Among NB samples, the  $i7$  showed the maximum enhancement of about 17.6-fold compare to the reference dye sample. The 99-fold enhancement was observed for sample  $i6$  with CF™620R dye.

The use of LBL technique gave us control over the minimum distances between AuNPs of the two arrays. However, there is a distribution of nanoparticle separations. In addition, the orientation of the fluorophores with respect to the nanoparticle and the glass surface is not controlled. Therefore, the observations represent an average over different AuNP-dye configurations.

In contrast to NB, no decrease of the fluorescence signal with respect to the reference sample was observed for CF™620R (figure S6 of the supplementary material<sup>68</sup> and Fig. 5) for thin barrier layers. As it is shown in Fig. 5, there is an increase in emission intensity by introducing thicker barrier layers (larger  $i$ ) and the maximum enhancement was achieved for  $i6$  corresponding to a 99-fold emission enhancement compared to the reference dye sample. For the samples with even thicker barriers, the emission intensity decreased. It should be noted that the stronger fluorescence signals for thicker PE layers cannot be explained simply by an increased number of dye molecules in these samples. In particular the results are presented relative to the reference dye sample which is prepared by the same method and with  $i = 5$ . The better performance of the CF™620R can be explained by its slightly smaller emission wavelength that is closer to the LSPR resonance. Although better enhancement is expected for dyes with smaller quantum yield<sup>69</sup>, here we need to consider the effect of better enhancement in absorption of the dye and near field coupling to AuNPs. However, a definite discussion is cumbersome since the emission spectra themselves are strongly tailored.

As shown in Fig. 6, the maximum of the emission spectrum ( $\lambda_{\text{Max}}$ ) shifts to the red by increasing the number of PE layers. This figure also shows that the shift does not depend on the excitation wavelength (same behaviors and values for CF<sup>TM</sup>620R double array samples under 550 nm and 590 nm excitation). The red-shift of the maximum emission and changes in the shape of emission spectra for fluorescence dyes near metallic particles have been reported for the case that the excitation laser and the dye emission overlap with the plasmon resonances.<sup>13,25,70</sup> The observed red shift of the plasmon resonances due to embedding (see figure S1 of the supplementary material<sup>68</sup>) shows a similar trend as a function of increasing the PE layer thickness, which indicates that these two phenomena are related. The shift of the emission peak maximum can be explained by a coupling of the dye's emission bands to the shifted plasmon resonance (cf. see figure S1 of the supplementary material<sup>68</sup>); the plasmonic system realizes a stronger interaction to different loss channels of the dyes depending on the electromagnetic properties of the sample.

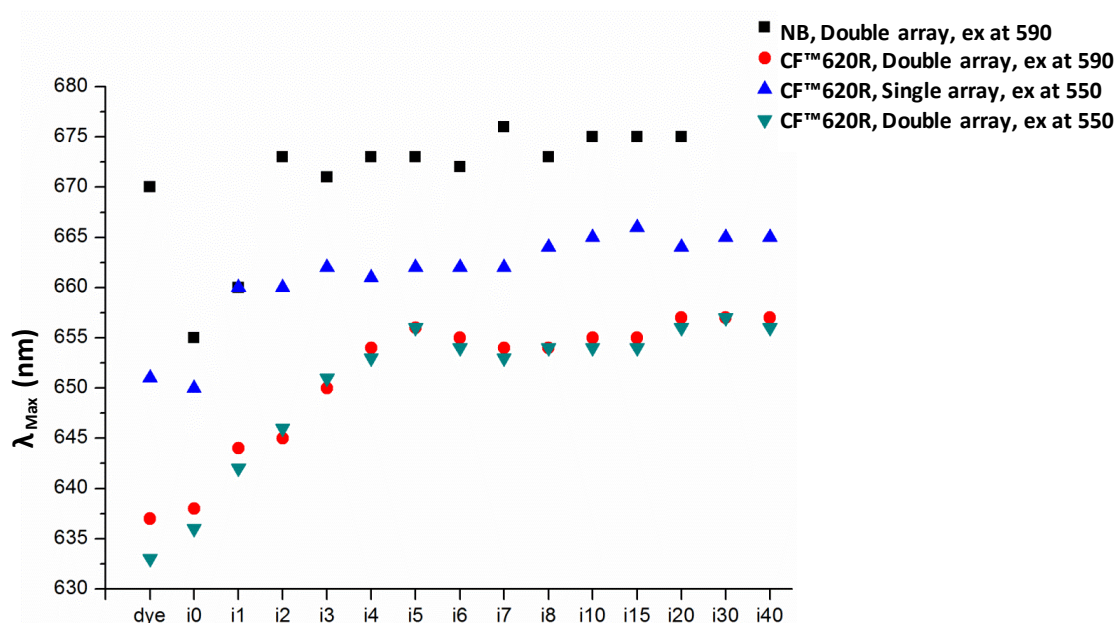


Fig. 6 Position of maximum emission spectra is presented for the single and double array of CF<sup>TM</sup>620R, and double array of samples with NB as a dye layer.

To study the phenomena in more detail, time-resolved fluorescence spectroscopy has been carried out under excitation at 590 nm for the samples with double array configuration. The lifetime for each sample was estimated by the deconvolution method using system identification toolbox of MATLAB R2014a which allows modelling and compensating disturbing effects. The results for CF<sup>TM</sup>620R double array configurations are presented in Fig. 7. The last samples with the thickest barrier layer (i20 and more) have a comparable average lifetime (about 2 ns) to the reference dye sample. There is a smooth increase of the lifetime by increasing the distance between the dye and the nanoparticle arrays. Thus, the maximum

fluorescence enhancement and minimum lifetime do not coincide. This behavior resulted from different phenomena: For small separations, the lifetime is strongly decreased. However, a coupling to nonradiative channels of the metallic particles is detrimental for the overall emission of the combined system. For larger separations, this quenching effect is less pronounced and a maximum in emission can be found despite an increased lifetime of the fluorophore.

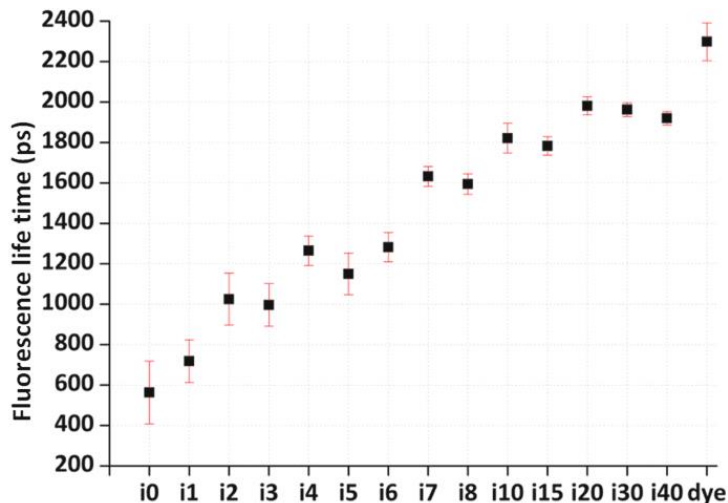


Fig. 7 Measured lifetimes for the double array CF<sup>TM</sup>620R samples with excitation at 590 nm. The values are averaged over four repeated measurements and the error bars represent the standard deviation.

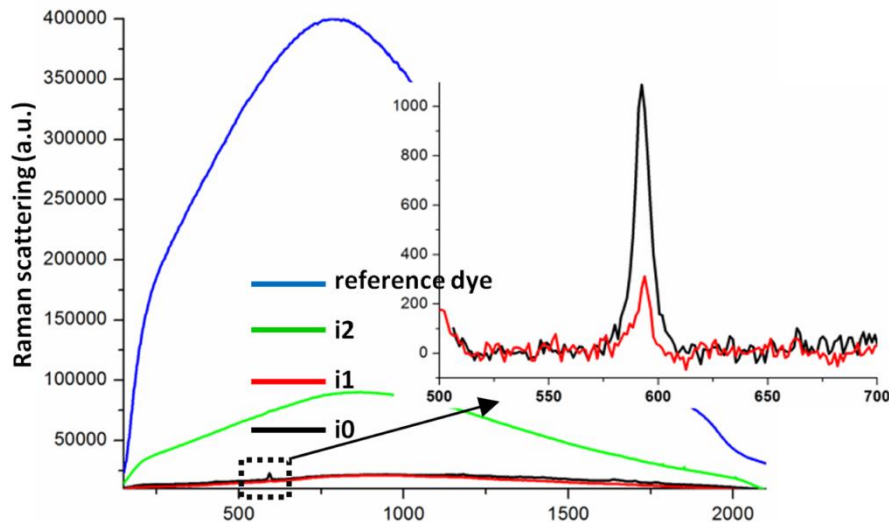


Fig. 8 Raman spectra with excitation at 633 nm for NB dye sample as a reference and i0, i1, and i2 samples with NB as a dye. By introducing more PE layers between the dye and AuNP arrays the distinct peak at 590 nm vanishes.

The experiments described earlier show the quite complex distance dependence of the fluorescence. Raman scattering is an instantaneous process and therefore quenching processes are not important. The distance dependence behavior should therefore be much simpler. The Raman scattering of the double array samples with NB dye as a Raman active fluorophore (Fig. 8) were measured by excitation at 633 nm, which can cause fluorescence as well.

We observed a broad fluorescence background for the dye sample. For the i0 sample, with only a single PE layer separating the dye and AuNP array, the distinct Raman peak of NB at 590 nm appeared, whereas the fluorescence background is low due to quenching. By increasing the separation between the dye layer and the nanoparticle arrays the Raman signal decreased (completely for i2) and the fluorescence background recovered. This measurement confirms the different distance dependencies of Raman and fluorescence enhancement and furthermore indicates that there is no significant diffusion of the dye through PE layer toward AuNP arrays.

#### IV. CONCLUSIONS

We investigated the fluorescence enhancement in the presence of single and double arrays of AuNPs with varying array distances. A tuning of the minimum distance between the closest particles and also the average distance between the dye layer and nanoparticle arrays was achieved with the LBL method. We observed a better enhancement for double array configurations. Furthermore, an optimal distance was identified with a 99-fold fluorescence enhancement in double array configuration. The minimum lifetime shortened 4 times compared to the reference dye sample for the sample with shortest dye to nanoparticle distance. Although an overall control of minimum distances is realized, the final measured enhanced emission is an average over emission of fluorophores with varying orientations and different distances from the nanoparticles. Our findings demonstrate that the overall thickness control with this method for double array configuration is sufficient to achieve enhancement factors up to 99-fold in NIR dye as CF<sup>TM</sup>620R.

#### ACKNOWLEDGMENTS

Financial support from University of Geneva and the Swiss National Science Foundation is acknowledged. This work was supported by the German Science Foundation within Project RO 3640/4-1. We would like to thank Bioimaging Center of University of Geneva for the access to electron microscopy.

#### REFERENCES

- <sup>1</sup> P. Biagioni, J. S. Huang, and B. Hecht, *Rep Prog Phys* **75**, 024402 (2012).
- <sup>2</sup> M. Bauch, K. Toma, M. Toma, Q. Zhang, and J. Dostalek, *Plasmonics* **9**, 781 (2013).
- <sup>3</sup> M. Chekini, P. Oulevey, and T. Burgi, *Current Applied Physics* **15**, 253 (2015).

- 4 J. Aizpurua, G. W. Bryant, L. J. Richter, F. J. G. de Abajo, B. K. Kelley, and T. Mallouk, *Physical Review B* **71** (2005).
- 5 D. J. de Aberasturi, A. B. Serrano-Montes, and L. M. Liz-Marzan, *Advanced Optical Materials* **3**, 602 (2015).
- 6 D. M. Yeh, C. F. Huang, C. Y. Chen, Y. C. Lu, and C. C. Yang, *Nanotechnology* **19** (2008).
- 7 S. Bishnoi, R. Das, P. Phadke, R. K. Kotnala, and S. Chawla, *Journal of Applied Physics* **116** (2014).
- 8 O. Kulakovich, N. Strekal, A. Yaroshevich, S. Maskevich, S. Gaponenko, I. Nabiev, U. Woggon, and M. Artemyev, *Nano Letters* **2**, 1449 (2002).
- 9 G. M. Akselrod, C. Argyropoulos, T. B. Hoang, C. Ciraci, C. Fang, J. N. Huang, D. R. Smith, and M. H. Mikkelsen, *Nature Photonics* **8**, 835 (2014).
- 10 J. R. Lakowicz, *Anal Biochem* **337**, 171 (2005).
- 11 S. Guddala, V. K. Dwivedi, G. V. Prakash, and D. N. Rao, *Journal of Applied Physics* **114** (2013).
- 12 J. R. Lakowicz, K. Ray, M. Chowdhury, H. Szmackinski, Y. Fu, J. Zhang, and K. Nowaczyk, *Analyst* **133**, 1308 (2008).
- 13 S. Khatua, P. M. Paulo, H. Yuan, A. Gupta, P. Zijlstra, and M. Orrit, *ACS Nano* **8**, 4440 (2014).
- 14 Q. Cui, F. He, L. Li, and H. Mohwald, *Adv Colloid Interface Sci* **207**, 164 (2014).
- 15 T. Ming, H. J. Chen, R. B. Jiang, Q. Li, and J. F. Wang, *Journal of Physical Chemistry Letters* **3**, 191 (2012).
- 16 E. Jang, K. J. Son, and W.-G. Koh, *Colloid and Polymer Science* **292**, 1355 (2014).
- 17 F. Caruso, K. Niikura, D. N. Furlong, and Y. Okahata, *Langmuir* **13**, 3422 (1997).
- 18 K. Aslan, J. R. Lakowicz, and C. D. Geddes, *Anal Bioanal Chem* **382**, 926 (2005).
- 19 K. Ray, R. Badugu, and J. R. Lakowicz, *J Phys Chem C Nanomater Interfaces* **111**, 7091 (2007).

- <sup>20</sup> A. De Luca, A. Iazzolino, J. B. Salmon, J. Leng, S. Ravaine, A. N. Grigorenko, and G. Strangi, *Journal of Applied Physics* **116** (2014).
- <sup>21</sup> N. Akbay, J. R. Lakowicz, and K. Ray, *J Phys Chem C Nanomater Interfaces* **116**, 10766 (2012).
- <sup>22</sup> P. Reineck, D. Gomez, S. H. Ng, M. Karg, T. Bell, P. Mulvaney, and U. Bach, *Acs Nano* **7**, 6636 (2013).
- <sup>23</sup> J. R. Lakowicz, Y. Shen, S. D'Auria, J. Malicka, J. Fang, Z. Gryczynski, and I. Gryczynski, *Anal Biochem* **301**, 261 (2002).
- <sup>24</sup> O. G. Tovmachenko, C. Graf, D. J. van den Heuvel, A. van Blaaderen, and H. C. Gerritsen, *Advanced Materials* **18**, 91 (2006).
- <sup>25</sup> M. Ringler, A. Schwemer, M. Wunderlich, A. Nichtl, K. Kurzinger, T. A. Klar, and J. Feldmann, *Phys Rev Lett* **100**, 203002 (2008).
- <sup>26</sup> K. Ray, R. Badugu, and J. R. Lakowicz, *Chem Mater* **19**, 5902 (2007).
- <sup>27</sup> S. Kuhn, U. Hakanson, L. Rogobete, and V. Sandoghdar, *Physical Review Letters* **97** (2006).
- <sup>28</sup> J. Zhang, Y. Fu, M. H. Chowdhury, and J. R. Lakowicz, *J Phys Chem C Nanomater Interfaces* **112**, 18 (2007).
- <sup>29</sup> M. H. Chowdhury, S. K. Gray, J. Pond, C. D. Geddes, K. Aslan, and J. R. Lakowicz, *Journal of the Optical Society of America B-Optical Physics* **24**, 2259 (2007).
- <sup>30</sup> J.-W. Liaw, C.-S. Chen, and J.-H. Chen, *Journal of Quantitative Spectroscopy and Radiative Transfer* **111**, 454 (2010).
- <sup>31</sup> S. Muhlig, D. Cialla, A. Cunningham, A. Marz, K. Weber, T. Burgi, F. Lederer, and C. Rockstuhl, *Journal of Physical Chemistry C* **118**, 10230 (2014).
- <sup>32</sup> O. Stranik, R. Nooney, C. McDonagh, and B. D. MacCraith, *Plasmonics* **2**, 15 (2006).
- <sup>33</sup> R. Bardhan, N. K. Grady, and N. J. Halas, *Small* **4**, 1716 (2008).
- <sup>34</sup> D. Cheng and Q. H. Xu, *Chem Commun (Camb)*, 248 (2007).

- 35 S. Damm, S. Fedele, A. Murphy, K. Holsgrove, M. Arredondo, R. Pollard, J. N. Barry, D. P. Dowling, and J. H. Rice, *Applied Physics Letters* **106** (2015).
- 36 N. N. Horimoto, K. Imura, and H. Okamoto, *Chemical Physics Letters* **467**, 105 (2008).
- 37 Y. M. Yu, M. Z. Yin, K. Mullen, and W. Knoll, *Journal of Materials Chemistry* **22**, 7880 (2012).
- 38 E. Jang, K. J. Son, and W. G. Koh, *Colloid and Polymer Science* **292**, 1355 (2014).
- 39 J. J. Mock, R. T. Hill, A. Degiron, S. Zauscher, A. Chilkoti, and D. R. Smith, *Nano Letters* **8**, 2245 (2008).
- 40 J. Malicka, I. Gryczynski, Z. Gryczynski, and J. R. Lakowicz, *Anal Biochem* **315**, 57 (2003).
- 41 Y. Cheng, T. Stakenborg, P. Van Dorpe, L. Lagae, M. Wang, H. Chen, and G. Borghs, *Anal Chem* **83**, 1307 (2011).
- 42 G. P. Acuna, F. M. Moller, P. Holzmeister, S. Beater, B. Lalkens, and P. Tinnefeld, *Science* **338**, 506 (2012).
- 43 Y. H. Zheng, L. Rosa, T. Thai, S. H. Ng, D. E. Gomez, H. Ohshima, and U. Bach, *Journal of Materials Chemistry A* **3**, 240 (2015).
- 44 F. Tam, G. P. Goodrich, B. R. Johnson, and N. J. Halas, *Nano Lett* **7**, 496 (2007).
- 45 C. Y. Jiang, S. Markutsya, and V. V. Tsukruk, *Langmuir* **20**, 882 (2004).
- 46 A. Cunningham, S. Muhlig, C. Rockstuhl, and T. Burgi, *Journal of Physical Chemistry C* **115**, 8955 (2011).
- 47 C. H. Zhang, J. Zhu, J. J. Li, and J. W. Zhao, *Journal of Applied Physics* **117** (2015).
- 48 S. Kadkhodazadeh, J. B. Wagner, H. Kneipp, and K. Kneipp, *Applied Physics Letters* **103** (2013).
- 49 A. Bek, R. Jansen, M. Ringler, S. Mayilo, T. A. Klar, and J. Feldmann, *Nano Lett* **8**, 485 (2008).
- 50 S. Pal, P. Dutta, H. N. Wang, Z. T. Deng, S. L. Zou, H. Yan, and Y. Liu, *Journal of Physical Chemistry C* **117**, 12735 (2013).

- 51 M. P. Busson, B. Rolly, B. Stout, N. Bonod, and S. Bidault, *Nature Communications* **3** (2012).
- 52 R. Gill and E. C. Le Ru, *Phys Chem Chem Phys* **13**, 16366 (2011).
- 53 D. Punj, J. de Torres, H. Rigneault, and J. Wenger, *Optics Express* **21**, 27338 (2013).
- 54 B. H. Lukas Novotny, *Principles of Nano-Optics* (Cambridge University Press, 2006).
- 55 M. P. Busson, B. Rolly, B. Stout, N. Bonod, J. Wenger, and S. B. Bidault, *Angewandte Chemie-International Edition* **51**, 11083 (2012).
- 56 K. Haberska and T. Ruzgas, *Bioelectrochemistry* **76**, 153 (2009).
- 57 A. Tronin, Y. Lvov, and C. Nicolini, *Colloid and Polymer Science* **272**, 1317 (1994).
- 58 P. Lavalle, C. Gergely, F. J. G. Cuisinier, G. Decher, P. Schaaf, J. C. Voegel, and C. Picart, *Macromolecules* **35**, 4458 (2002).
- 59 G. Decher, *Science* **277**, 1232 (1997).
- 60 X. Zhang, C. A. Marocico, M. Lunz, V. A. Gerard, Y. K. Gun'ko, V. Lesnyak, N. Gaponik, A. S. Susha, A. L. Rogach, and A. L. Bradley, *ACS Nano* **6**, 9283 (2012).
- 61 M. Lunz, A. L. Bradley, W. Y. Chen, V. A. Gerard, S. J. Byrne, Y. K. Gun'ko, V. Lesnyak, and N. Gaponik, *Physical Review B* **81** (2010).
- 62 J. Turkevich, P. C. Stevenson, and J. Hillier, *Discussions of the Faraday Society*, 55 (1951).
- 63 H. Q. Zheng, C. B. Gao, and S. N. Che, *Microporous and Mesoporous Materials* **116**, 299 (2008).
- 64 J. Kimling, M. Maier, B. Okenve, V. Kotaidis, H. Ballot, and A. Plech, *J Phys Chem B* **110**, 15700 (2006).
- 65 S. Muhlig, C. Rockstuhl, J. Pniewski, C. R. Simovski, S. A. Tretyakov, and F. Lederer, *Physical Review B* **81** (2010).
- 66 P. B. Johnson and R. W. Christy, *Physical Review B* **6**, 4370 (1972).
- 67 D. J. Zahniser and J. F. Brenner, *Cytometry* **6**, 392 (1985).

<sup>68</sup> See supplemental material at [URL will be inserted by AIP] for additional information; the maximum of extinction peaks vs. number of applied PE layers (S1), the fluorescence emission spectra of single gold nanoparticle array (S2) and double array samples (S3) of CF<sup>TM</sup>620R dye with excitation at 550 nm, the extinction spectra of double array samples with the NB dye (S4), the fluorescence emission spectra of the double array samples with NB as a dye layer with excitation at 590 nm (S5), fluorescence emission spectra of the double array samples with CF<sup>TM</sup>620R as a dye layer with excitation at 590 nm (S6) and the normalized decay curves of CF<sup>TM</sup>620R double array samples at S7.

<sup>69</sup> H. Aouani, O. Mahboub, E. Devaux, H. Rigneault, T. W. Ebbesen, and J. Wenger, *Nano Letters* **11**, 2400 (2011).

<sup>70</sup> T. Ming, L. Zhao, Z. Yang, H. J. Chen, L. D. Sun, J. F. Wang, and C. H. Yan, *Nano Letters* **9**, 3896 (2009).